top of the waveguide and the buried oxide layer, and less than ~$3\times10^{-3}$ between the waveguide sidewalls. The attenuation bandwidth has been determined under both small and large signal drive conditions. This is shown in Fig. 6, where the measured small signal attenuation bandwidth is plotted as a function of attenuation. It can be seen that the small signal modulation bandwidth increases with the static attenuation level. The time to set a given attenuation level is also shown on the secondary axis. The turn-on time of the device is dependent on the attenuation level being set, which is itself a function of the voltage applied to the device. Transient simulations have also been carried out to investigate the factors limiting the modulation bandwidth of the attenuator, and these simulations compared with device measurements. The turn-off speed of the EVOA is found to increase with higher levels of bias attenuation because of decreasing carrier lifetimes at higher carrier densities. The experimentally observed 10%-90% fall times in switching off the attenuation increased from 70 ns to 150 ns for attenuation changes from 30 dB to 0 dB and 0.8 dB to 0 dB respectively. However the 10%-90% risetimes decreased from 160 ns to 60 ns for the same respective attenuation swings of 0 to 30 dB and 0 to 0.8 dB.

In summary we have described the use of a novel waveguide taper for the reduction of insertion loss in a four-channel, highly efficient, high-speed integrated EVOA. This demonstrates the potential for high level, low loss, multifunctional integration of the EVOA with other functionalities such as arrayed waveguide gratings (AWG) using the same manufacturing process. This ability to integrate multiple functions onto a single chip is crucial in developing multi-function devices which are smaller, more efficient and cheaper to manufacture in volume than their discrete counterparts.

**References**

[1] R.A. Soref and B.R. Bennett, IEEE J. Quantum Electron. **QE-23,** 123 (1987).
[2] I.E. Day, A.A. House, J. Drake and M. Asghari, Proc. NFOEC 2001 p.943.
[3] M. Asghari and E.J.C. Dawney, Proc. SPIE **3620,** 252 (1999).
[4] "ATLAS User's Manual: Device Simulation Software," Silvaco Data Systems International, Version 1.5.0 (April 1997).

## TuN 4:30 PM - 6:00 PM
B313B-B314

### Wavelength Multiplexing and Switching

Randy Giles, *Lucent, USA,Presider*

**TuN1** **4:30 PM**

### A Surface and Bulk Micromachined Angular Vertical Combdrive for Scanning Micromirrors

W. Piyawattanametha, P. Patterson, M. Wu, *Department of Electrical Engineering, University of California, Los Angeles, CA;* D. Hah, *ETRI, Daejeon, Republic of Korea;* H. Toshiyoshi, *University of Tokyo, Tokyo, Japan, Email: wibool@icsl.ucla.edu.*

We present a high performance scanning micromirror with angular vertical comb actuators realized by combining MUMPs with a 3-mask deep-reactive-ion-etching post process. A DC scan angle of ±4° (mechanical) is achieved at 40V.

**1. Introduction**

Micro-electro-mechanical (MEM) mirrors have wide applications in dense wavelength-division-multiplexed (DWDM) components, including optical crossconnect, wavelength-selective switches, reconfigurable optical add-drop multiplexers, and optical attenuators [1]. The surface-micromachining technology is very attractive for small micromirrors because of its design flexibility, similarity to integrated circuit (IC) process, and well-established foundry service. It has been used successfully in several commercial products such as projection display [2] and 2D MEMS switches [3]. Bulk-micromachining technology, on the other hand, offers large, stress-free single crystalline mirrors and more powerful, comb-based actuators [4-6]. However, electrical interconnect is a major challenge due to the lack of conformal layers in silicon-on-insulator (SOI)-based MEMS, particularly for more sophisticated devices such as 2D arrays of 2D scanners. An integrated surface/bulk micromachining process that combines the benefits of both is highly desirable. Some progress has been made in previous reports [7-9].

In this paper, we report on a scanning micromirror with angular vertical comb (AVC) actuators fabricated by a new surface/bulk micromachining process. We have developed a simple, 3-mask post process to add high-aspect-ratio single-crystalline silicon (SCS) structures to fully processes MUMPs (Multi-User MEMS Processes provided by Cronos) chips or wafers. Scanners with 40-um-thick micromirrors and angular vertical comb fingers have been successfully fabricated. The scanner has a diameter of 1 mm, a DC scan angle of ± 4° (mechanical) at 40 V bias, and a resonant frequency of 661 Hz. The radius of curvature of the mirror is 55 cm.

**2. Micromirror Design**

The schematic drawing of the AVC scanner is illustrated in Fig. 1a. A single crystalline micromirror is suspended by a pair of polysilicon torsion springs and actuated by AVC drives. The scanner has 4 comb banks with 12 movable fingers each. The finger is 4 um wide, 150 um long, and 40 um thick. The gap spacing between comb fingers is 3 um. The torsion spring is 500 um long, and the micromirror is 1000 um in diameter and 40 um thick. Compared with other vertical comb devices [4, 5], the AVC has a simpler fabrication process (it requires only a single layer of SCS) and is completely self-aligned [6]. It also has larger scan range. Though AVC can be realized by bulk-micromachining alone [6], the combined surface/bulk micromachining process offers additional flexibilities in mechanical design and electrical interconnect. Electrically isolated SCS islands can be mechanically joined together by the surface-micromachined structures. The SCS islands can be individually addressed by polysilicon lines. Complex wiring is possible with 3 level interconnect. The surface-micromachined structures are fabricated using MUMPs. All critical mechanical structures are defined in the MUMPs layout, including the comb patterns, micromirrors, torsion springs, electrical bias lines, and polysilicon latching structures. We have developed a simple 3-mask post process to convert the SCS substrate into mechanical structures. The metal pattern in MUMPs process is used as the mask for deep reactive ion etching (DRIE) of vertical combs and micromirrors. Polysilicon spring latches and keyholes fix the initial angles of the angular vertical combs precisely (Fig. 1b).

**3. Fabrication**

The fabrication process is outlined in Fig. 2a. The surface-micromachined structures are fabricated using the MUMPs services, while the 3-mask bulk-micromachining process was performed at UCLA. The MUMPs wafer is first thinned down

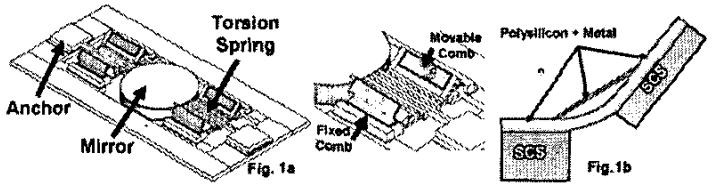


Fig. 1a: Schematic drawing of a micromirror. Inset shows the details of a micromirror. Fig. 1b: Schematic cross section drawing of a comb finger.

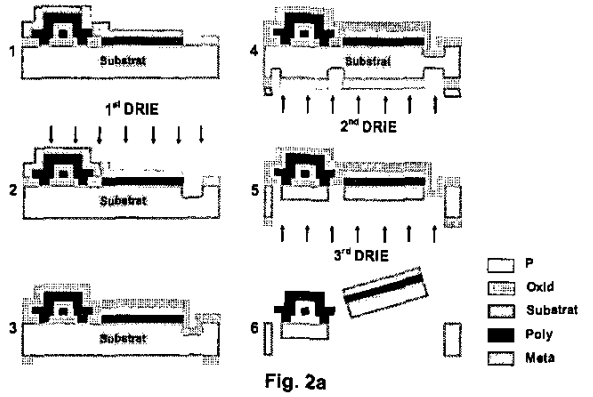


Fig. 2a

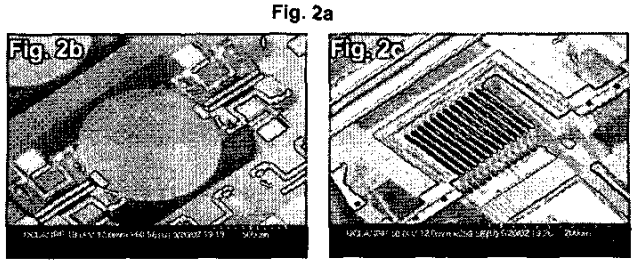


Fig. 2a: Fabrication process of a micromirror. Fig. 2b: SEM of a AVC scanning micromirror. Fig. 2c: A closed-up SEM of the angular comb.

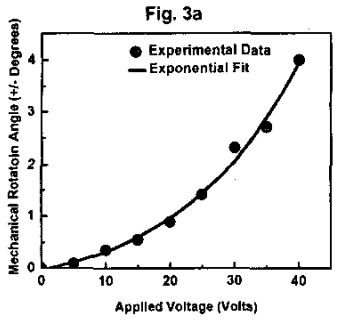


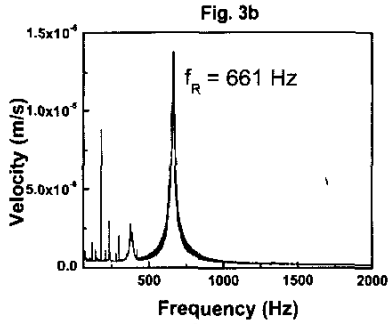


Fig. 3a: DC transfer curve of a micromirror. Fig. 3b: Frequency response of the AVC scanner.

to 350 um. The backside is polished to avoid micromasking effect. The comb fingers and the micromirrors are etched by DRIE using the gold pattern in MUMPs as the etching mask. The polysilicon hinges are protected by photoresist during etching (Mask 1). After etching, the front side is protected by a 1-um-thick PECVD oxide. Then, a 3-um-thick PECVD oxide is deposited on the backside. The area underneath the mirror and the combs is opened using a double-side aligner, Karl Suss MA-6 (Mask 2). The third mask defines the SCS islands from the backside. A shallow etch is performed to delineate the SCS areas. Then, the photoresist is removed, and the backside substrate is left with the previously patterned oxide. The third DRIE completely removes the substrate between the SCS islands. Etching continues until it stops on phosphorous silicate layer 1 (PSG1) of the MUMPS chip. The device is then released in 49% HF for 40 minutes and dried in an oven at 110°C. The angular comb fingers are assembled manually to a pre-defined angle and locked in place by polysilicon latches. The SEM of the scanning micromirror with angular vertical comb-drive is shown in Fig. 2b. Fig. 2c is a close-up view of one corner of the micromirror showing the supporting 40 um thick bulk SCS underneath the comb finger.

**3. Experiment Result**

The DC scanning characteristics is shown in Fig. 3a. A mechanical scan angle of ± 4° has been achieved at a bias voltage of 40 V. Larger scan angle can be achieved with larger initial tilting angle of the angular comb and/or thicker comb fingers. Lower voltage can be achieved with larger number of comb fingers. The dynamic response (Fig. 3b) is measured using a Polytec Vibrascan Polytec Vibrascan Laser Doppler Vibrometer. A sharp resonance at 661 Hz is observed. The mirror curvature and the surface roughness are characterized by a WYKO RST 500 Optical Profiler. The radius of curvature for the mirror is found to be 55 cm. The mirror flatness can be further improved by using thicker SCS layer. The surface roughness is measured to be 12 nm.

**4. Conclusion**

We have successfully demonstrated a high performance scanning micromirror using a combined surface/bulk micromachining process. Large scan angle (± 4° mechanical) and low operating voltage (40 V) are achieved for 1-mm-diameter scanners. The resonant frequency is 661 Hz. The proposed process can be directly extended to 2D scanners where more complex electrical interconnect is required.

**5. Reference**

[1]. D. Bishop, V. Aksyuk, C. Bolle, R. Giles, F. Pardo, and J. Walker, "MEMS/MOEMS for lightwave networks: can little machines make it big?," Proceedings of the SPIE - The International Society for Optical Engineering, **Vol.4175**, SPIE-Int. Soc. Opt. Eng, 2000, pp. 2-5.

[2]. L. J. Hornbeck, "Deformable-Mirror Spatial Light Modulators," Spatial Light Modulators and Applications III, SPIE Critical Reviews, **Vol. 1150**, Aug 1989, pp. 86-102.

[3]. L. Fan, S. Gloeckner, P. D. Dobblelaere, S. Patra, D. Reiley, C. King, T. Yeh, J. Gritters, S. Gutierrez, Y. Loke, M. Harburn, R. Chen, E. Kruglick, M. Wu, and A. Huasain, "Digital MEMS switch for planar photonic crossconnects," OFC 2002, pp. 93-94.

[4]. R. A. Conant, J. T. Nee, K. Y. Lau, and R. S. Muller, "A Flat High - Frequency Scanning Micromirror," Solid - State Sensor and Actuator Workshop, Hilton Head Island, SC, USA, Jun. 2000, pp. 6-9.

[5]. U.Krishnamoorthy, and O. Solgaard, "Self - aligned vertical comb drive actuators for optical scanning micromirrors," MOEMS 2001.

[6]. P. Patterson, D. Hah, H. Chang, H. Toshiyoshi, and M.C. Wu, "An Angular Vertical Comb Drive Actuator for Scanning Micromirrors," MOEMS 2001.

[7]. J. L. Yeh, H. Jiang, and N. C. Tien, "Integrated polysilicon and DRIE bulk silicon micromachining for an electrostatic torsional actuator," Journal of Microelectromechanical Systems, **Vol.8, No.4**, IEEE, Dec. 1999, pp. 456-65.

[8]. H. Xie, Y. Pan, and G. K. Fedder, "A SCS CMOS Micromirror for Optical Coherence Tomographic Imaging," MEMS 2002, pp. 495-498.

[9]. G-D. J. Su, H. Toshiyoshi, and M. C. Wu, "Surface-micromachined 2-D optical scanners with high-performance single-crystalline silicon micromirrors," IEEE Photonics Technology Letters, **Vol.13, No.6**, IEEE, June 2001, pp. 606-8.

**TuN2** **4:45 PM**

## Widely Tunable, Narrow Optical Bandpass Gaussian Filter Using a Silicon Microactuator

J. Berger, F. Ilkov, D. King, A. Tselikov, D. Anthon, *Iolon, Inc., San Jose, CA, Email: jberger@iolon.com.*

A Littrow diffraction grating Gaussian bandpass optical filter uses a silicon microactuator to tune over 40nm with narrow bandwidth, 2dB insertion loss, 0.2dB PDL, ±20ps/nm dispersion, fast tuning, and accurate wavelength control in a compact butterfly package.

**1. Introduction**

Widely tunable lasers and filters are being deployed in dense wavelength division multiplexing (DWDM) networks for applications ranging from multi-wavelength sparing and inventory reduction via universal line cards, to dynamic wavelength provisioning in reconfigurable transparent optical networks [1]. Tunable filters offer wavelength flexibility at the receiver analogous to the use of tunable lasers at the transmitter. Tunable filter applications include tunable receivers, ASE suppression, optical performance monitoring, and signal demultiplexers for broadcast-and-select architectures. We have implemented a novel tunable filter design which meets demanding performance requirements for optical network applications in a small form factor, environmentally robust package. The filter is based on a micro-optical Littrow diffraction grating and beam expander combined with a silicon microactuator for mechanical tuning, all assembled in a hermetic butterfly package. Optical devices using silicon microactuators require low-mass moving parts such as silicon micromirrors to optimize speed and range of motion. While traditional Littrow monochromators tune by grating rotation, the microactuator-grating filter tunes by reflecting light from a rotating silicon micromirror to change the beam incidence angle at the grating. The optics are designed to maintain a constant filter bandwidth as the mirror rotates across the tuning range. High efficiency diffraction gratings optimized for a single polarization state have inherently high polarization dependent loss (PDL). The insertion loss and PDL of the microactuator-grating filter are minimized using a co-packaged micro-optical circulator to impart light of a single polarization state on the grating. The microactuator-grating filter offers several performance advantages compared to other widely tunable filter technologies such as fiber Bragg grating [2], thin film dielectric [3,4], and fiber Fabry-Perot [5]. The filter supports full C or L band tuning and narrow bandwidths for high out-of-band channel rejection at 25, 50, or 100 GHz channel spacing with a wide range of bandwidths achievable using the same optical components. The filter has low insertion loss and PDL, low dispersion enabling use at 10 Gb/s data rates, and accurate wavelength control. Adaptive wavelength tracking to the incoming signal in combination with an ultra-narrow, matched Gaussian filter passband also offers new possibilities for improved DWDM system performance.

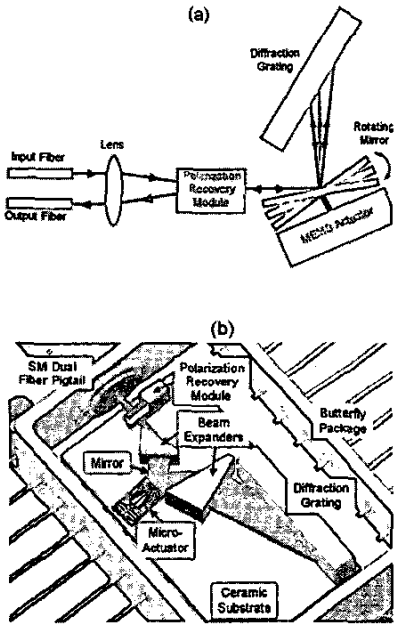


Fig. 1. (a) The Littrow diffraction grating tunable filter center wavelength is selected by the mirror angle, which determines the wavelength of the diffracted light returning to the center of the output fiber. (b) The micro-optics and silicon microactuator are assembled on a common substrate mounted in a hermetically sealed butterfly package.

**2. Filter design**

The widely tunable filter shown in Fig. 1 is a miniature monochromator based on a free space Littrow diffraction grating, an anamorphic prism pair beam expander, and a silicon microactuator. The collimated beam from a single mode input fiber passes through a polarization recovery module (PRM), reflects from a mirror mounted on a microactuator, and diffracts from a 95% efficiency, Littrow-mounted diffraction grating. The PRM is a micro-optical circulator consisting of a polarizing beam splitter, Faraday rotator, and two half-wave plates. The PRM minimizes polarization dependent loss (PDL) and polarization mode dispersion (PMD) in the filter by converting the randomly polarized input light into p-polarized light incident at the grating, and then circulating